Gas–Liquid Two-Phase Flow Through Packed Beds in Microgravity

Brian J. Motil
NASA Glenn Research Center, Cleveland, OH 44135

Vemuri Balakotaiah
Dept. of Chemical Engineering, University of Houston, Houston, TX 77204

Yasuhiro Kamotani
Dept. of Mechanical and Aerospace Engineering, Case Western Reserve University, Cleveland, OH 44106

Experimental data on flow pattern transitions, pressure drop, and flow characteristics for cocurrent gas–liquid flow through packed columns in microgravity is analyzed. The pulse flow regime exists over a wider range of gas and liquid flow rates under microgravity conditions. Furthermore, maps used to predict transition boundaries in normal gravity do not apply in microgravity. The flow regime data are compared to the widely used Talmor map and a new transition criterion between bubble and pulse flow in microgravity is proposed. The pressure-drop data clearly show that interfacial effects can increase the pressure drop by as much as 300% compared to those predicted by the single-phase Ergun equation. A two-phase friction factor is correlated to the superficial gas and liquid Reynolds numbers and the Suratman number. New data are also presented on the influence of gravity on the pulse amplitude and frequency.

Introduction

In the typical operation of a packed-bed reactor, gas and liquid flow simultaneously through a fixed bed of solid particles. Depending on the application, the particles can be various shapes and sizes and serve to force the two fluid phases through the narrow channels connecting the interstitial space. This configuration provides for intimate contact and high rates of transport between the phases needed to sustain chemical or biological reactions. The packing may also serve as either a catalyst or as a support for growing biological material.

The packed-bed reactor is relatively compact and requires minimal power to operate. This makes it an excellent candidate as a potential unit operation in support of long-duration human space activities. In the literature, the effects of gravity on flow-regime maps are either neglected or do not correctly scale to the microgravity environment (Charpentier and Favier, 1975; Chou et al., 1977; Midoux et al., 1976; Sato et al., 1973; Tosun, 1984; Weekman and Myers, 1964; and Talmor, 1977). Furthermore, it is not clear whether the pressure-drop correlations developed for normal gravity applications and, based on the Lockhart and Martinelli (1949) approach (which ignores interfacial tension and gravity), can be applied to microgravity conditions, especially when inertial effects are not dominant. There are also fundamental differences between the flow patterns in normal and microgravity conditions. For example, trickle flow and countercurrent flow cannot exist in microgravity, because they rely on gravity to drive one of the fluids. In addition, there is no free-draining, liquid holdup which, in microgravity, prohibits the direct use of pressure-drop correlations developed for normal-gravity packed beds based on internal holdup (Larkins et al., 1961; Midoux et al., 1976; Satterfield, 1975; Tosun, 1984). By examining the relative role of forces other than gravity that contribute to the hydrodynamics of a packed-bed reactor, a better understanding of terrestrial applications is also possible. In normal-gravity cocurrent downflow of a gas and liquid, it is very difficult to measure the true frictional pressure drop since it is coupled to the hydrostatic head; which depends on the dynamic gas and liquid holdup. Under microgravity conditions, the pressure drop measured is the true frictional pressure drop.

Correspondence concerning this article should be addressed to B. J. Motil.

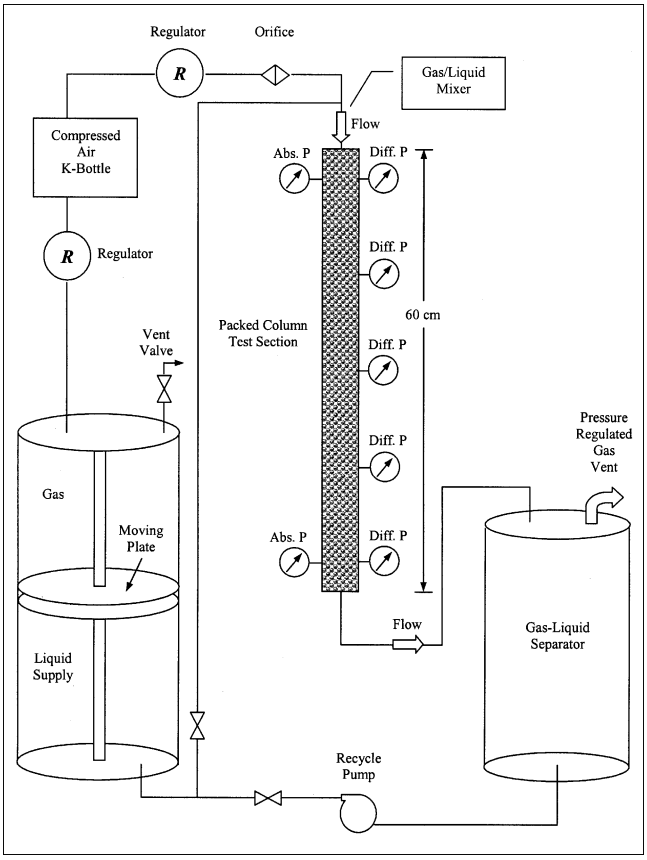

Figure 1. Experimental setup.

Experimental System

A simplified flow view of the experimental apparatus is illustrated in Figure 1. The experiment was designed to fly on NASA's KC-135 aircraft, which is capable of flying parabolic trajectories to create a reduced-gravity environment for approximately 20 s. Acceleration levels were recorded in three mutually orthogonal axes (one coinciding with the direction of flow) and typically averaged less than 0.01 m/s^2 during the 20-s "low-g" period. Gas was provided to the test section by a compressed-air cylinder and was controlled by regulating the pressure upstream of an orifice. Two different sized orifices were selected to maintain choked flow conditions for all flow rates and were verified with a mass flowmeter before each test day. Liquid flow was maintained by applying air pressure to a piston, which in turn forced the liquid through a meter and into the test section. A pressure-driven piston, rather than a pump, is necessary during low gravity to ensure steady liquid flow. The two phases were mixed prior to the test section and then introduced into the column through a coarse-mesh screen. To maintain a steady pressure at the outlet of the test section, a two-phase separator/collector tank was used to retain the liquid phase while venting the gas (air) to the cabin via a back-pressure regulator. Average pressures within the packed-bed test section were held between 100 and 200 kPa. Between trajectories, the liquid was pumped back to the supply tank.

A clear rectangular polycarbonate column with a cross section of 2.54 cm by 5.08 cm and 60 cm long was used for the test section. Five flush-mounted differential pressure transducers were spaced at even intervals with the first location approximately 4 cm from the inlet port and the subsequent pressure transducers spaced at 13-cm intervals along the column. In addition, absolute pressure transducers were located at the first and last positions. To observe pulse formation and characteristics adequately, the data from the differential pressure transducers was acquired at 1,000 Hz. Flow rates, temperatures, and absolute pressures were recorded at 1 Hz. Visual observations were recorded using a high-speed SVHS video system at 500 frames per second. The column was randomly packed with spherical glass beads of identical diameter by slowly dropping the beads into the top of the bed. Handling and shaking the bed was kept to a minimum prior to the aircraft flights, but the vibration and alternating 0 to 1.8-g environment created a more tightly packed bed. The void fraction was measured by comparing the dry weight to the weight of the bed filled with water (recorded after the flight). Typically, the beads settled after only several parabolas, leaving a gap of about 2 to 3 cm on the top of the column. The average void fraction was found to be 0.345. This was slightly lower than the normal range of 0.36 to 0.43 reported in Kaviany (1995), but is consistent with the findings of Tosun (1984).

The experiments were designed to provide variations of several orders-of-magnitude in the important dimensionless numbers and were obtained by varying the packing size, gas and liquid flow rates, and the liquid viscosity (by using water–glycerin solutions). The ranges of flow rates, fluid properties, packing diameters, and dimensionless numbers are summarized in Table 1. Over 250 different test conditions were evaluated along with a companion set of tests in normal gravity for direct comparison. Additional experimental details are provided in Motil et al. (2001).

Flow Regimes in Normal and Microgravity

It is well known that four basic flow regimes can exist in cocurrent gas–liquid flow through packed beds in normal gravity for nonfoaming systems. Each regime has very distinct hydrodynamic characteristics which affect the heat- and mass-transfer rate, pressure drop, and liquid holdup. Weekman and Myers (1964), Charpentier and Favier (1975), Sato et al. (1973), and Ng (1986) provide detailed descriptions of each regime that include two so-called low-interaction

Table 1. Range of Parameters and Dimensionless Numbers

Parameter	Range
L	3–50 kg/m^2 s
G	0.03–0.8 kg/m^2 s
ρ_L	1,000–1,200 kg/m^3
ρ_G	0.95–2.3 kg/m^3
μ_L	0.001–0.02 kg/m·s
μ_G	1.8×10^{-5} kg/m·s
σ_L	0.060–0.072 kg/s^2
d_P	0.002 and 0.005 m
ϵ	0.345
Re_{LS}	7–300
Re_{GS}	8.5–175
We_{LS}	4.1×10^{-4}–0.19
Su_L	900–365,000

regimes (bubbly and trickle) and two high-interaction regimes (pulse and spray). The level of interaction refers to the mixing between phases and strongly influences mass and heat transfer.

As stated in the Introduction, trickle flow, which is characterized by the liquid phase flowing down over the packed material as a falling film driven almost entirely by gravity, does not exist in microgravity. This was verified in our experiments by observing that the liquid phase would simply pool under the flow conditions that would result in trickle flow in normal gravity and instead be a very slow bubbly flow. Spray flow, which occurs at very high gas-to-liquid ratios, is characterized by liquid droplets entrained in the packing by the highly turbulent gas flow. The high inertia of the denser liquid phase dominates so that the gravity force has little influence on the hydrodynamic characteristics of the flow. In our comparisons of zero vs. normal gravity conditions, we observed almost no noticeable differences in pressure drop or flow-regime transitions for spray flow. On the other hand, pulse flow (characterized by alternating gas-rich and liquid-rich regions) and dispersed bubble flow (characterized by gas bubbles dispersed throughout the continuous liquid phase) are both influenced by gravity and are the focus of this work. Steady countercurrent flow conditions cannot occur in microgravity since, in the absence of any other driving force, both phases will flow in the direction of the favorable pressure gradient.

Initially, we compared both our normal and microgravity experimental results with Talmor's (1977) flow-regime map. Although others are available, Talmor's map was selected because it is widely accepted and has an explicit gravity term. Talmor develops a driving-to-resistance force ratio for two-phase flow through a packed column similar to two-phase flow through an empty tube. The driving forces are inertia and gravity, while the resistance forces are viscous and surface tension. By normalizing the inertia forces and defining the Froude, Weber, and Reynolds numbers in terms of the gas/liquid mixture properties (indicated here by an overhead bar), Talmor derives the force ratio

$$\frac{\text{Inertia}+\text{gravity}}{\text{Interface}+\text{viscous}}=\frac{1+\left(1/\overline{Fr}\right)}{\left(1/\overline{We}\right)+\left(1/\overline{Re}\right)} \tag{1}$$

Equation 1 did not provide a well-defined boundary for the pulse flow regime, so Talmor argued that the relative effect of viscosity and surface tension were not the same. The dynamic "interface" force was redefined as (inertia force)^2/surface tension, and Eq. 1 becomes

$$\frac{\text{Inertia}+\text{gravity}}{\text{Dynamic interface}+\text{viscous}}=X=\frac{1+\left(1/\overline{Fr}\right)}{\overline{We}+\left(1/\overline{Re}\right)} \tag{2}$$

The two-phase dimensionless groups are defined as

$$\overline{We}=\frac{D^*\left(L+G\right)^2\nu_{LG}}{\sigma} \tag{3}$$

$$\overline{Re}=\frac{D^*\left(L+G\right)}{\mu_{LG}} \tag{4}$$

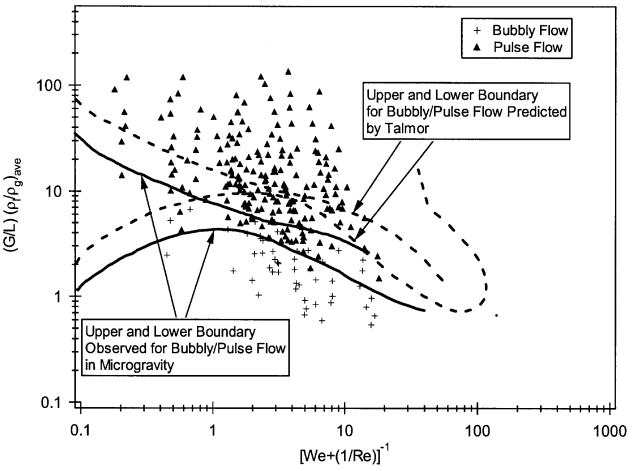

Figure 2. Comparison of flow regimes in microgravity to Talmor map.

$$\overline{Fr}=\frac{\left[\left(L+G\right)\nu_{LG}\right]^2}{gD^*} \tag{5}$$

where

$$\nu_{LG}=\nu_L\frac{L/G}{1+L/G}+\nu_G\frac{1}{1+L/G} \tag{6}$$

$$\mu_{LG}=\mu_L\frac{L/G}{1+L/G}+\mu_G\frac{1}{1+L/G} \tag{7}$$

$$D^*=\frac{2\epsilon D_h}{2+3(1-\epsilon)(D_h/d_P)} \tag{8}$$

As expected, our normal gravity (vertical downflow) results agreed with the Talmor map reasonably well. This also helped confirm that our definition of pulse flow was similar to that used by Talmor and those he referenced.

Using the same experiment and transition criteria, we then plotted our microgravity results on the Talmor map in Figure 2. The same dimensionless parameters were used noting that the gravity term $(1/\overline{Fr})$ can now be neglected. The data clearly show that the bubble-to-pulse transition occurs at a much lower volumetric gas-to-liquid ratio than predicted by Talmor. This may be a result of the hydrostatic pressure restraining the interfacial activities in normal gravity flow or the underestimation of the capillary forces by this flow-regime map. The gas–liquid interface appears to be much more active in microgravity than in normal gravity. Capillary forces enhance the formation and amplitude of the pulse pressure wave, and are discussed in more detail later.

New flow-regime map for microgravity

For two-phase flows in microgravity, an approach to mapping flow pattern transitions was recently developed by one of the authors and can be applied to the packed bed as well (Jayawardena et al., 1997). Assuming that both phases are incompressible and the flow is quasi-steady and fully developed, the variables influencing the hydrodynamics are the re-

spective liquid and gas superficial velocities (U_{LS}, U_{GS}), viscosities (μ_L, μ_G) and densities (ρ_L, ρ_G), as well as the interfacial tension (σ), the packing diameter (d_P), the gravitational acceleration (g), and the bed inclination (θ). In general, for nonspherical particles, the sphericity is also a parameter. Likewise, the bed porosity may also influence the flow pattern. However, in our experiments, only uniform spherical particles were used, and for random packing the porosity is nearly constant at 0.345.

The number of variables influencing the flow pattern can be immediately reduced by two with the removal of gravity, which consequently leads to an inherent symmetry in the bed so that θ is no longer relevant either. Making use of the Buckingham–Pi theorem (with length, mass, and time as reference dimensions), five independent dimensionless parameters can be written to characterize the two-phase flow through a packed bed

$$Re_{GS} = \frac{\rho_G U_{GS} d_P}{\mu_G} \tag{9}$$

$$Re_{LS} = \frac{\rho_L U_{LS} d_P}{\mu_L} \tag{10}$$

$$We_{LS} = \frac{\rho_L U_{LS}^2 d_P}{\sigma} \tag{11}$$

$$\frac{\rho_G}{\rho_L} \tag{12}$$

$$\frac{\mu_G}{\mu_L} \tag{13}$$

Since the gas-to-liquid density and viscosity ratios are both on the order of 10^{-3} and 10^{-2}, respectively, we expect the transition boundaries to be a weak function of these two ratios (if their magnitude does not change significantly). Rearranging the three most relevant dimensionless groups such that one group is dependent only on fluid and bed properties, we obtain the Suratman number

$$Su_L = \frac{Re_{LS}}{Ca_{LS}} = \frac{Re_{LS}^2}{We_{LS}} = \frac{d_P \rho_L \sigma}{\mu_L^2} \tag{14}$$

It is worth noting that the Suratman number is the reciprocal squared of the Ohnesorge number, which arises in the analysis of capillary effects in small-diameter tubes and jets.

Using the ratio of the gas-to-liquid Reynolds numbers as the other coordinate in our microgravity flow-regime map, the results shown in Figure 3 indicate the importance of the Suratman number in determining the transition from bubble to pulse flow. Although the surface tension and liquid densities did vary slightly in our experiments, each Suratman number shown here essentially represents a unique combination of liquid viscosity and packing size. With these two variables, we were able to span a range of Suratman numbers by three orders of magnitude ($10^2 < Su_L < 10^5$). For each Suratman number, there exists a particular value for the ratio of Reynolds numbers (Re_{GS}/Re_{LS}) where the transition occurs.

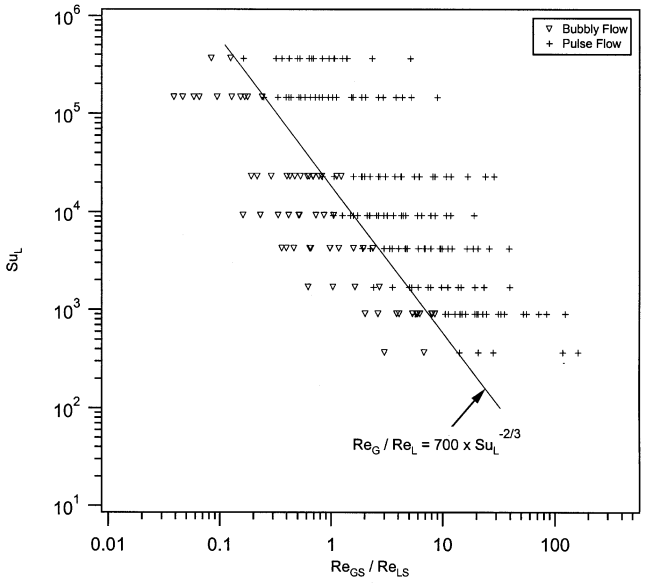

Figure 3. Bubble-pulse transition for microgravity conditions.

The transitional value decreases with increasing Su_L

$$\left(\frac{Re_{GS}}{Re_{LS}}\right)_{\text{tran}} = KSu_L^{-2/3} \tag{15}$$

where the numerical value of K is found to be 700. We note that this relation has a striking similarity with the bubble–slug transition in tubes without packing, where K was found to be 464 (Jayawardena et al., 1997). This suggests a similar transition mechanism.

The flow-transition map in Figure 3 assumes that for a given Su_L, the transition is not a function of Re_{LS}. We verified this assumption by plotting Re_{LS} as the dependent variable in Figure 4. Although Re_{LS} varies by two orders of magnitude, the transition boundary is shown to be a very weak function of Re_{LS} (or Re_{GS}) and depends only on the ratio.

Bubble – pulse transition mechanism

The "transition" to pulse flow from either dispersed bubble or trickle flow is typically defined as the first visible onset of a pulse near the bottom of the column (Sato et al., 1973; Ng, 1986). The flow is considered "pulse flow" after the pulse has traversed over the entire column. Unfortunately, the pulse never fully spans the length of the column, so the point of fully developed pulse flow is somewhat arbitrary. Nevertheless, this definition is used throughout the literature.

To ensure that our transition points were consistent with previous works, we ran our entire test matrix in normal gravity. We found that the most concise technique for identifying the flow pattern in our experiments was to monitor the pressure transducer located about 17 cm from the exit (or bottom). We also focused the high-speed video camera on this location, with a wide field of view spanning ± 15 cm from the transducer location. Once the flow was developed and a flow regime established, we zoomed the video to a field of view of

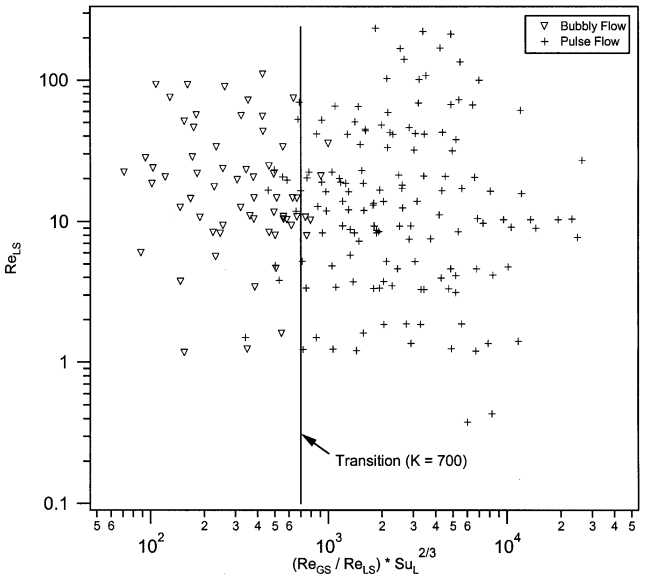

Figure 4. Effect of superficial liquid Reynolds number (Re_{LS}) on bubble-pulse transition.

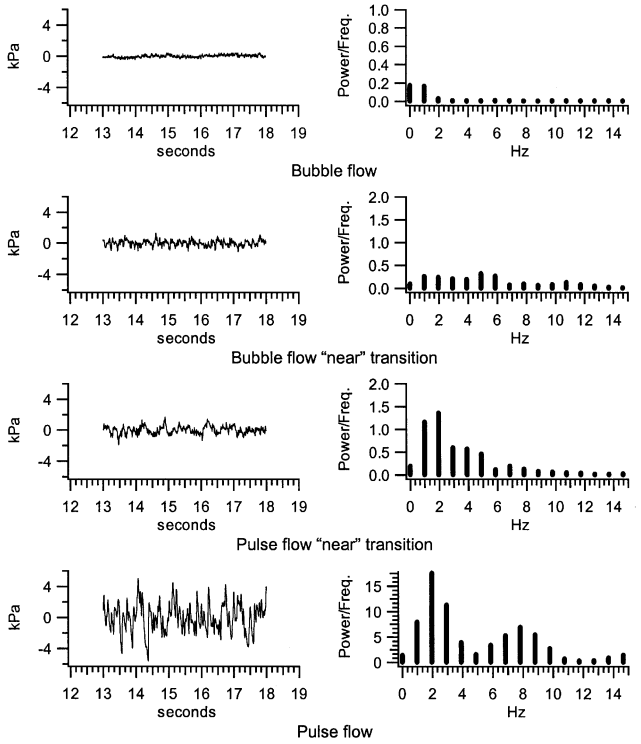

Figure 5. Pressure trace and power spectral density (PSD) plots for 2 mm, $\mu_L = 0.001$ kg/m·s.

2 to 3 cm to observe pore-level flow conditions. As expected, the pulse formation in microgravity also started near the exit of the column and moved upstream as the gas flow rate was increased. A fast Fourier transform (FFT) analysis was performed on the pressure fluctuations based on a commercially available prime factor multidimensional algorithm. Figure 5 shows the corresponding power spectrum density (PSD) plot along with the actual pressure trace for a representative case using 2-mm beads with pure water. As the gas flow is increased to just prior to the onset of any visible pulse formations, the pressure transducers begin to indicate pressure fluctuations with a frequency content somewhat spread out over the first 15 Hz. The first distinct frequency (around 2 Hz) is evident as soon as pulse flow begins to form. Finally, once full pulse flow is established throughout the column, two characteristic frequencies at 2 and 8 Hz are clearly present. Using the PSD to determine the flow regime with a high-speed video as a confirmation, we found our normal gravity transitions to be in good agreement with Talmor (1977), Tosun (1984), and (for the pure water case) Charpentier and Favier (1975).

Observing these phenomena in microgravity is advantageous because the bubble–pulse transition occurs at a much lower liquid flow rate as well as a lower volumetric gas–liquid ratio than in normal gravity. This enables a much clearer visualization. When the gas is introduced at a low flow rate, the discrete bubbles tend to flow in relatively straight lines; that is, a rectilinear motion, in the direction of the bulk flow (similar to flow in a channel without packing; Taitel et al., 1980). Much like the case without packing, there is little interaction between the bubbles at these flow conditions. However, unlike an empty channel, the bubbles are continuously flowing through alternating constricting and expanding pores and, as the gas flow rate is increased, the single bubbles begin to coalesce with neighboring bubbles much earlier than at similar superficial velocities in a channel without packing. It is at this point that we begin to see small pulses forming (typically over 10% to 20% of the width of the bed).

Pressure Drop

A considerable number of models and correlations have been proposed over the years to predict pressure drop and liquid saturation in packed-bed reactors. The general approach is to either develop a phenomenological model based on macroscopic force balances or to develop a purely empirical correlation. The recent article by Pinna et al. (2001) provides a literature survey of both types.

The most commonly used models based on macroscopic force balances generally involve a modification to an Ergun-type equation and, when extended to two-phase flows, are typically applicable only to the low-interaction (trickle flow) regime where the gas phase is continuous and the hydrostatic head can be neglected. Furthermore, pressure drop associated with the dynamic interaction between the phases is minimal. Some examples include models proposed by Sweeney (1967), Saez and Carbonell (1985), Holub et al. (1993), and Al-Dahhan et al. (1998). Rao et al. (1985) proposed an Ergun-type model for pressure drop in cases other than trickle flow, but each model is restricted to a specific flow regime (dispersed bubble or pulse) with errors of $\pm 30\%$ for the pulse regime. The model of Rao et al. also requires a good estimate of the dynamic liquid holdup.

Many empirical models are also available in the literature, most derived from either the Lockhart and Martinelli-type parameters or some other set of dimensionless parameters. Lockhart and Martinelli-type parameters, such as those pro-

posed by Larkins et al. (1961), Midoux et al. (1976), Tosun (1984), and Pinna et al. (2001), are based on the physical model of separated flow. Each phase is considered separately and the resulting pressure drop assumed to be entirely due to friction losses, that is, surface tension is neglected. Most of these models require an accurate estimate of liquid holdup or a term based on the averaged fluid density to account for the hydrostatic pressure resulting from the liquid phase. Other empirical models based on dimensionless parameters, such as the gas and liquid Reynolds numbers (Specchia and Baldi, 1977) or the liquid Reynolds and Weber numbers (Larachi et al., 1991), are also available, but these correlations either neglect the effects of gravity or are valid under only very specific operating conditions, such as high pressure.

Effect of gravity on pressure drop

Gravity effects on total pressure drop cannot be neglected for the bubble or pulse flow regimes. Figure 6 shows a direct comparison of identical flow rates for both normal and microgravity. In the bubble flow regime, the difference between the two gravity environments varies linearly and is approximately equivalent to the liquid static head. As the gas flow is increased and pulse flow begins, the difference in pressure drop begins to decrease as the inertia forces begin to dominate the flow. The difference becomes negligible in the spray flow regime.

Under normal gravity cocurrent downflow, the purely frictional contribution to the pressure drop cannot be measured directly. The dynamic holdup of the gas and liquid must be determined to resolve the hydrostatic contribution to the pressure change. This can be accomplished by cleverly designed experiments (such as simultaneously closing the inlet and exit valves and determining the mass of gas and liquid trapped) or through various correlations reported in the literature. Unfortunately, different investigators report substantially different results. Thus, the 1-*g* pressure-drop data reported in the literature (especially in the bubble and pulse flow regimes) are masked by errors of undetermined magnitude due to the static contribution. In the microgravity environment, the hydrostatic head is eliminated, which allows for the direct measurement of the frictional pressure drop.

Validity of the Lockhart – Martinelli correlation in microgravity

From the many correlations available based on Lockhart–Martinelli coordinates, the Tosun model was selected because it has been shown to work well in normal gravity for most types of packing (Pinna et al., 2001). Tosun used the Ergun equation to determine the single-phase pressure drop with $\alpha = 118.2$ and $\beta = 1.0$ for spherical glass beads.

As expected, our normal gravity data are shown in Figure 7a to be in good agreement with Tosun's correlation. The $\pm 14\%$ limits given in Tosun's results, which represent 92% of the measured pressure drop, are shown as dashed lines.

The scatter is much greater with the microgravity data (Figure 7b), and there is an upward shift in the measured pressure drop. The shift upward was expected, because the hydrostatic pressure gradient is eliminated. Although not shown, it is interesting to note that the original constants

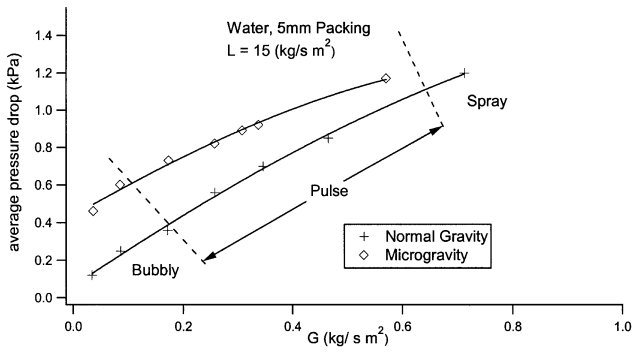

Figure 6. Average pressure drop for normal and microgravity conditions.

proposed by Ergun (1952) ($\alpha = 150$ and $\beta = 1.75$) would provide a much better fit for our microgravity data; however, it does not change the amount of scatter. This is because Ergun used only the gas phase to calculate his constants, so his results where not influenced by the static pressure. The increase in scatter is a good indication of the degree to which the capillary or surface-tension effects are masked by the hydrostatic head.

Model for frictional pressure drop in microgravity

As mentioned earlier, modified Ergun models have worked reasonably well by restricting use to the gas–continuous

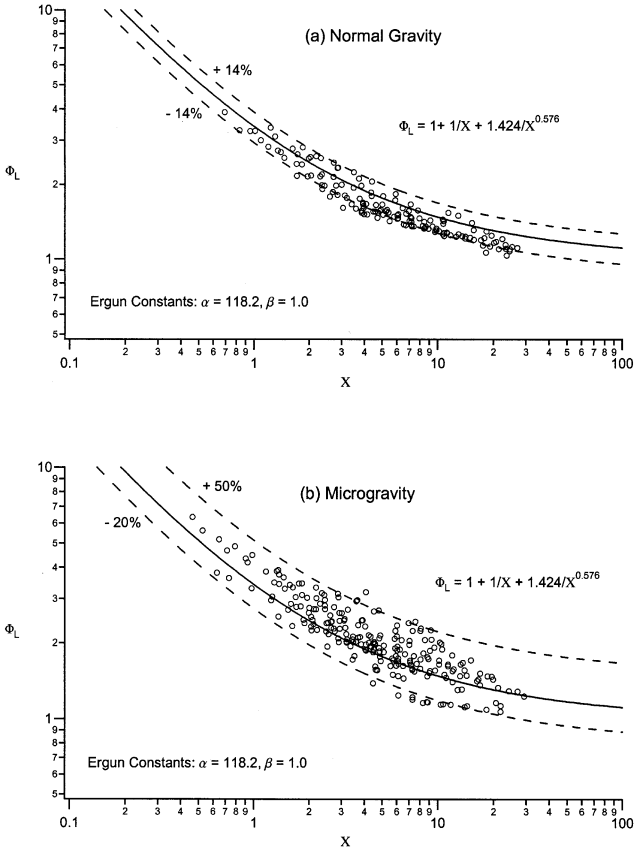

Figure 7. Lockhart–Martinelli plot based on Tosun's correlation.

regime and neglecting the effects of gravity and phase interaction. We propose a new model of the same form for bubble and pulse flow by adding a term for the dynamic phase interaction that can be validated in the microgravity environment without determining the dynamic liquid holdup.

Following the same type of dimensional arguments used in developing our flow-regime transition map, the pressure drop over the length of the column can be written as a function of the following

$$\frac{-\Delta P}{Z} = f[U_{LS}, U_{GS}, \mu_L, \mu_G, \rho_L, \rho_G, \sigma, d_P, \epsilon] \qquad (16)$$

Using the Buckingham–Pi theorem, Eq. 16 can be written in terms of the dimensionless two-phase pressure drop.

$$\frac{-\Delta P}{Z}\frac{d_P}{\rho_L U_{LS}^2} = f\left[\frac{\rho_G}{\rho_L}, \frac{\mu_G}{\mu_L}, \frac{\sigma}{\rho_L U_{LS}^2 d_P}, \frac{\mu_L}{\rho_L U_{LS} d_P}, \frac{U_{GS}\rho_G d_P}{\mu_G}, \epsilon\right] \qquad (17)$$

As reasoned earlier, we again ignore the weak dependence on the density and viscosity ratios and write Eq. 17 in terms of the following dimensionless groups

$$\frac{-\Delta P}{Z}\frac{d_P}{\rho_L U_{LS}^2} = f\left[\frac{1}{We_{LS}}, \frac{1}{Re_{LS}}, Re_{GS}, \epsilon\right] \qquad (18)$$

Recognizing that the Weber number can be represented in terms of the liquid Reynolds number and the Suratman number, which comprises only fluid and bed properties (that is, no velocities)

$$\frac{1}{We_{LS}} = \frac{Su_L}{(Re_{LS})^2} \qquad (19)$$

Equation 18 can be written in terms of the gas and liquid Reynolds numbers for a fixed set of packed-bed conditions

$$\frac{-\Delta P}{Z}\frac{d_P}{\rho_L U_{LS}^2} = f\left[\frac{Su_L}{Re_{LS}^2}, \frac{1}{Re_{LS}}, Re_{GS}, \epsilon\right] \qquad (20)$$

Equation 20 must meet the following three criteria (limiting cases): (1) in the limit of zero interfacial tension between fluids ($\sigma \approx 0$), it should reduce to the single-phase Ergun equation; (2) in the limit of no gas flow ($Re_{GS} = 0$), it should again reduce to the single-phase Ergun equation; (3) in the inertia-dominated limit ($Re_{LS} \gg 1$), the friction factor should become independent of the interfacial tension and viscous terms. Based on these considerations, the form of the dynamic phase interaction term is

$$f_{TP} - f_{SP} = \gamma\left(\frac{Re_{GS}}{1-\epsilon}\right)^a\left(\frac{1-\epsilon}{Re_{LS}}\right)^b\left(\frac{(1-\epsilon)^2 Su_L}{Re_{LS}^2}\right)^c \qquad (21)$$

Figures 8 and 9 show the experimental data and a fit of Eq. 21 with the single-phase terms added (which do not change the form of Eq. 20). Determining the parameter values $a = 1/2$, $b = 1/3$, $c = 2/3$, and $\gamma = 0.8$ by regression, Eq. 21 can be written in its final form as a modified Ergun equation with a dynamic phase interaction term

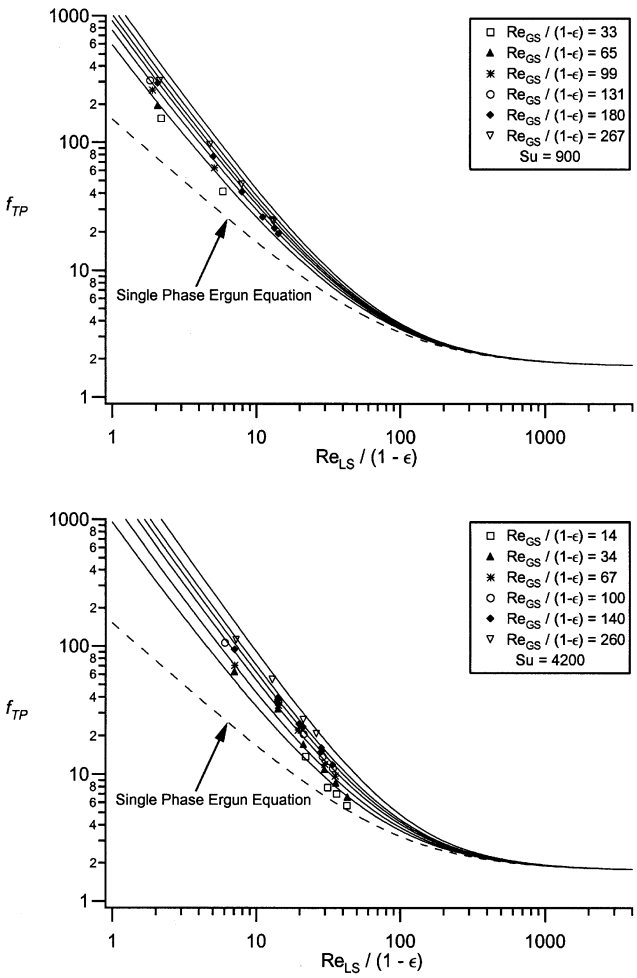

Figure 8. Modified two-phase Ergun equation for lower Suratman numbers.

$$f_{TP} = \frac{-\Delta P}{Z}\frac{d_P}{\rho_L U_{LS}^2}\frac{\epsilon^3}{1-\epsilon} = \frac{1-\epsilon}{Re_{LS}}\left[180 + 0.8\left(\frac{Re_{GS}}{1-\epsilon}\right)^{1/2}\left(\frac{Su_L(1-\epsilon)}{Re_{LS}}\right)^{2/3}\right] + 1.8 \qquad (22)$$

For the limiting cases (1) and (2), this term goes to zero. For case (3), both the viscous and dynamic phase-interaction terms go to zero. Using Eq. 22, a plot can be generated for each Suratman and gas Reynolds number. The constant γ is a function of the bed porosity, but since the porosity in our experiments was constant at 0.345, we cannot determine the exact functional dependence of γ on ϵ. The scatter in the correlation given by Eq. 22 is much smaller than that for any existing correlation for normal gravity two-phase pressure drop. As stated earlier, the main reason for the large scatter in 1-g data is due to the error involved in estimating the static head.

Experimental error was relatively small, so error bars are not shown in Figures 8 and 9. An analysis of the propagated error resulted in $\pm 6.1\%$ for the two-phase friction factor

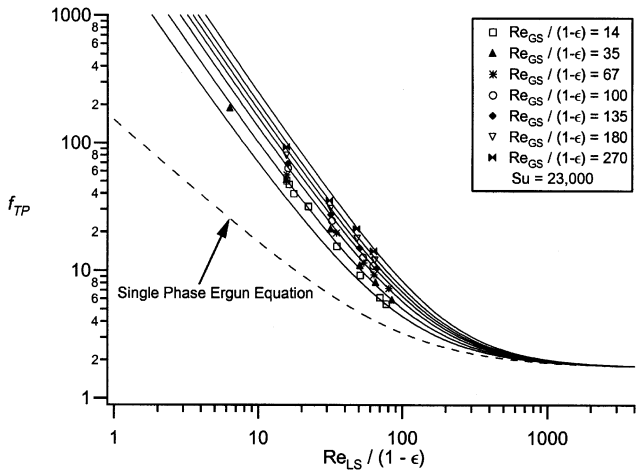

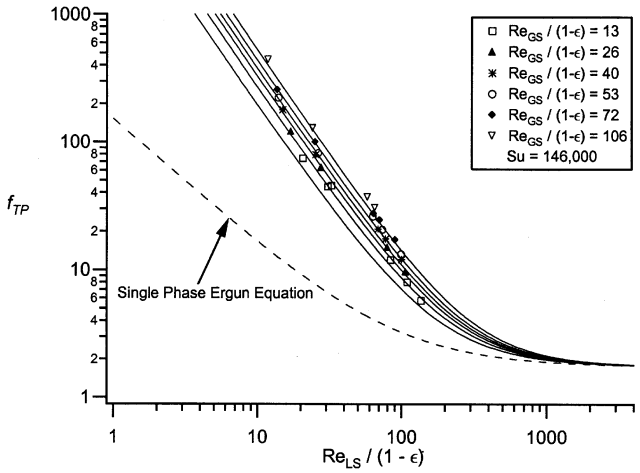

Figure 9. Modified two-phase Ergun equation for higher Suratman numbers.

(f_{TP}) and $\pm 5.4\%$ for the modified liquid Reynolds number (Re_{LS}).

Equation 22 is applicable for estimating the true frictional pressure drop only in the bubble and pulse flow regimes. It does not have the correct functional form to predict the pressure drop in the spray flow regime (or in the limit of the liquid volume fraction going to zero).

The minimum modified gas Reynolds number reached in our experiments was 13. At this value of $Re_{GS}/(1-\epsilon)$, the two-phase friction factor predicted by our correlation is much higher (by a factor of 3 to 10) than the single-phase value. However, within the range of our experiments, the friction factor varied only by a factor of 2 to 3. The range of gas flow rates not covered by our experiments ($Re_{GS}/(1-\epsilon) < 13$) is larger than the range covered here, especially at the higher values of the Suratman number. Equation 22 will be validated further by new experiments with very low gas flow rates in the bubbly flow regime.

Another important issue not addressed by our experiments is the influence of the inlet pressure on the two-phase pressure drop, that is, whether the pressure drop depends on the gas volumetric flow rate or Reynolds number. We have chosen to correlate the friction factor to Re_{GS} rather than the gas volumetric flow rate for two reasons: first, at a fixed mass flow rate, Re_{GS} remains constant even if the inlet pressure changes. Second, dimensional arguments (and analogy with single-phase flow) lead us to use dimensionless groups such as Re_{GS}.

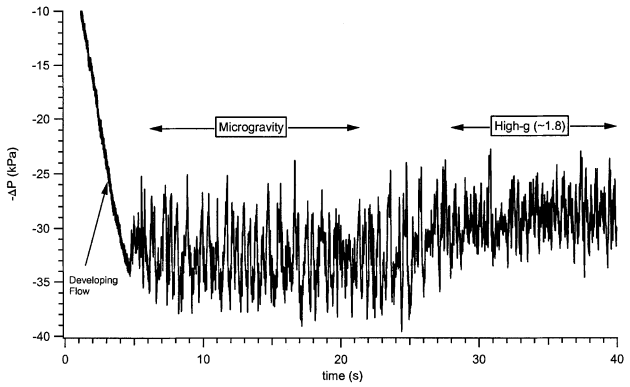

Figure 10. Typical pressure trace for pulse flow in low and high gravity.

Effect of Gravity on Pulse Characteristics

Many of the differences between normal and microgravity two-phase gas–liquid flow through packed beds can be explained by examining the effect of gravity on the pulse amplitude and frequency. Figure 10 illustrates the pressure trace for a typical pulse flow in which we continued to record the trace beyond the microgravity segment of the aircraft trajectory. As the aircraft begins to pull out of the microgravity dive, the experiment is subjected to an increased downward acceleration of 1.8 times that of normal gravity. From this pressure trace, it can be seen clearly that the average pressure drop shifts because of a change in hydrostatic head. In addition, the pulse amplitude decreases during the high-gravity (1.8-g) period. As the gravity level increases, the liquid film surrounding the particles drains faster and the wave amplitude at the gas–liquid interface decreases. This observation provides insight into the apparent shift of the flow regime transitions seen in the Talmor map.

A shift in pulse frequency can also be observed as the pulse flow transitions to the higher gravity. In the example trace shown, the dominant frequency shifts from a range of 1 Hz to 2 Hz (for microgravity) to a range of 2 Hz to 3 Hz (for high gravity). We only obtained these types of data (that is, we recorded pressure during the high-g pullout) for four cases, but observed a similar shift (usually about double) in each case. Additional experiments of this type are planned for future work.

Conclusions and Discussion

In this article, we have presented the first experimental data on flow regimes and pressure drop for gas–liquid two-phase flows through packed beds in microgravity. The experimental results presented here lead to two important conclusions. First, the flow regimes and the transitions that exist in microgravity are different than those in normal gravity. Second, the frictional pressure drop (which can be measured accurately under microgravity conditions) is much higher than

that for single-phase flow (liquid only), and is a strong function of the interfacial tension. We have used the data to propose a modified friction-factor correlation for gas–liquid flow through packed beds in the bubbly and pulse flow regimes. Preliminary data on the influence of gravity on the pulse amplitude and frequency are also presented. This work also demonstrates the utility of microgravity (and high-gravity) experiments in the understanding of normal gravity multiphase flows. For example, we can modify Eq, 22 to include the hydrostatic contribution in normal gravity and obtain a more accurate form of the Ergun equation valid for gas–liquid cocurrent downflow through packed beds. These extensions will be pursued in future work.

Acknowledgments

This work was supported by a grant from the National Aeronautics and Space Administration (Grant #NAG3-2697). The work of V. Balakotaiah was partially supported by the Institute for Space Systems Operations at University of Houston.

Notation

Ca_{LS} = superficial liquid capillary number
d_p = diameter of packing
D_h = hydraulic diameter of the empty bed
D^* = hydraulic diameter of bed as defined in Eq. 8
f_{SP} = single-phase friction factor
f_{TP} = two-phase friction factor
Fr = Froude number
G = superficial mass velocity of gas
g = gravitational constant
L = superficial mass velocity of liquid
Re_{GS} = superficial gas Reynolds number
Re_{LS} = superficial liquid Reynolds number
Su_L = Suratman number based on liquid properties
U_{GS} = superficial gas velocity
U_{LS} = superficial liquid velocity
We_{LS} = superficial liquid Weber number
Z = length of column

Other

$\overline{(\ )}$ = based on phase averages defined by Talmor, Eqs. 2 to 7

Greek letters

$-\Delta P$ = average pressure drop
ϵ = void fraction (fraction of space in column not occupied by packing)
μ_G = gas viscosity
μ_L = liquid viscosity
μ_{LG} = phase-averaged viscosity, Eq. 7
ν_{LG} = phase-averaged specific volume, Eq. 6
θ = bed inclination with respect to horizontal plane
ρ_G = gas density
ρ_L = liquid density
σ = liquid surface tension

Literature Cited

Al-Dahhan, M. H., M. R. Khadilkar, Y. Wu, and M. P. Dudukovic, "Prediction of Pressure Drop and Liquid Holdup in High-Pressure Trickle-Bed Reactors," *Ind. Eng. Chem. Res.*, **37**, 793 (1998).

Charpentier, J. C., and M. Favier, "Some Liquid Holdup Experimental Data in Trickle-Bed Reactors for Foaming and Nonfoaming Hydrocarbons," *AIChE J.*, **21**, 1213 (1975).

Chou, T. S., F. L. Worley, and D. Luss, "Transition to Pulsed Flow in Mixed-Phase Cocurrent Downflow Through a Fixed Bed," *Ind. Eng. Chem. Process Des. Dev.*, **16**, 424 (1977).

Ergun, S., "Fluid Flow Through Packed Columns," *Chem. Eng. Prog.*, **48**, 89 (1952).

Holub, R. A., M. P. Dudukovic, and P. A. Ramachandran, "Pressure Drop, Liquid Holdup, and Flow Regime Transition in Trickle Flow," *AIChE J.*, **39**, 302 (1993).

Jayawardena, S. S., V. Balakotaiah, and L. C. Witte, "Flow Pattern Transition Maps for Microgravity Two-Phase Flows," *AIChE J.*, **43**, 1637 (1997).

Kaviany, M., *Principles of Heat Transfer in Porous Media*, 2nd ed., Springer-Verlag, New York (1995).

Larachi, F., A. Laurent, N. Midoux, and G. Wild, "Experimental Study of Trickle-Bed Reactor Operating at High Pressure: Two-Phase Pressure Drop and Liquid Saturation," *Chem. Eng. Sci.*, **46**, 1233 (1991).

Larkins, R. P., R. R. White, and D. W. Jeffrey, "Two-Phase Cocurrent Flow in Packed Beds," *AIChE J.*, **7**, 231 (1961).

Lockhart, R. W., and R. C. Martinelli, "Proposed Correlation of Data for Isothermal Two-Phase Two-Component Flow in Pipes," *Chem. Eng. Prog.*, **45**, 39 (1949).

Midoux, N., M. Favier, and J. C. Charpentier, "Flow Pattern, Pressure Loss and Liquid Holdup Data in Gas-Liquid Downflow Packed Beds with Foaming and Nonfoaming Hydrocarbons," *J. Chem. Eng., Jpn.*, **9**, 350 (1976).

Motil, B. J., V. Balakotaiah, and Y. Kamotani, "Effects of Gravity on Cocurrent Two-Phase Gas-Liquid Flows Through Packed Columns," AIAA Aerospace Sciences Meeting (2001).

Ng, K. M., "A Model for Flow Regime Transitions in Cocurrent Down-Flow Trickle-Bed Reactors," *AIChE J.*, **32**, 115 (1986).

Pinna, D., E. Tronconi, and L. Tagliabue, "High Interaction Regime Lockhart-Martinelli Model for Pressure Drop in Trickle-Bed Reactors," *AIChE J.*, **47**, 19 (2001).

Rao, V. G., and A. A. H. Drinkenburg, "A Model for Pressure Drop in Two-Phase Gas-Liquid Downflow Through Packed Columns," *AIChE J.*, **31**, 1010 (1985).

Saez, A. E., and R. G. Carbonell, "Hydrodynamic Parameters for Gas-Liquid Cocurrent Flow in Packed Beds," *AIChE J.*, **31**, 52 (1985).

Satterfield, C. N., "Trickle-Bed Reactors," *AIChE J.*, **21**, 209 (1975).

Sato, Y., F. Takahashi, and Y. Hashiguchi, "Flow Pattern and Pulsation Properties of Cocurrent Gas-Liquid Downflow in Packed Beds," *J. Chem. Eng., Jpn.*, **6**, 315 (1973).

Specchia, V., and G. Baldi, "Pressure Drop and Liquid Holdup for Two Phase Concurrent Flow in Packed Beds," *Chem. Eng. Sci.*, **32**, 515 (1977).

Sweeney, D. E., "A Correlation for Pressure Drop in Two Phase Concurrent Flow in Packed Beds," *AIChE J.*, **13**, 663 (1967).

Taitel, Y., D. Bornea, and A. E. Dukler, "Modeling Flow Pattern Transitions for Steady Upward Gas-Liquid Flow in Vertical Tubes," *AIChE J.*, **26**, 345 (1980).

Talmor, E., "Two-Phase Downflow Through Catalyst Beds," *AIChE J.*, **23**, 868 (1977).

Tosun, G., "A Study of Cocurrent Downflow of Nonfoaming Gas-Liquid Systems in a Packed Bed: 1. Flow Regimes: Search for a Generalized Flow Map; 2. Pressure Drop: Search for a Correlation," *Ind. Eng. Chem. Process Des. Dev.*, **23**, 29 (1984).

Weekman, V. W., and J. E. Myers, "Fluid-Flow Characteristics of Concurrent Gas-Liquid Flow in Packed Beds," *AIChE J.*, **10**, 951 (1964).

Manuscript received Mar. 25, 2002, and revision received Sept. 4, 2002.